EVALUATION OF FLOW CONDITIONS DOWNSTREAM OF A TURBOFAN PROPULSION SIMULATOR FAN STAGE

M. Berens, E. Goldhahn

Airbus, Germany

Keywords: turbofan propulsion simulator, intake distortions, OGV flow

ABSTRACT

Turbofan propulsion simulators (TPS) are employed in wind tunnel tests to simulate the mutual effects between engines and airframe. TPS fan thrust is derived from gas path measurements in the fan duct downstream the fan stage. Some advanced aircraft concepts come with inherently higher intake distortions which influence these measurements. A wind tunnel test has been performed with an isolated TPS configuration to characterise the flow conditions downstream of a TPS fan stage in detail utilizing a rotational rake traversing device. Various configurational and operational parameters were varied in an experimental parametric study. Sensitivities of the flow conditions with respect to the parameters varied have been determined.

NOMENCLATURE

Latin Symbols

A19 [m²]	Fan nozzle exit area
DM19is [kg/s]	Isentropic fan mass flow rate
F19is [kg/s]	Isentropic fan gross thrust
i [-]	Index
M0 [-]	WT freestream Mach number
n [-]	Sample size
P_{ref} [N/m²]	Reference pressure: 101325 N/m²
P0 [N/m²]	WT freestream static pressure
PT0 [N/m²]	WT freestream total pressure
PT15 [N/m²]	Fan stage exit total pressure
r [m]	Radius
R [J/(kg·K)]	Gas constant = 287.05 J/(kg·K)
RPM [min-1]	Rotational speed
T_{ref} [K]	Reference temperature: 288.15 K
TT0 [K]	WT freestream total temperature
TT15 [K]	Fan stage exit total temperature
V19is [m/s]	Isentropic fan jet velocity

Subscripts

c0	… upstream wind tunnel conditions corrected parameter
rot	… rotating rake
fix	… (simulated) fixed rake

Greek Symbols

α [deg]	Angle of attack
α_3 [deg]	Fan OGV air outlet angle
α'_3 [deg]	Fan OGV trailing edge metal angle
θ [deg]	Rotating rake azimuth position angle
$\Delta\theta$ [deg]	Fan OGV wake azimuthal deviation
$\theta_{fr,wt}$ [deg]	Simulated fixed rake azimuth angle
γ [-]	Ratio of specific heats = 1.4

Abbreviations

BLSWT	Airbus Bremen Low-Speed WT
BLI	Boundary Layer Ingestion
BM	Bellmouth Intake
ECF	Engine Calibration Facility
FI	Flight Intake
FPR	Fan (Total) Pressure Ratio
IR	Infra-Red (Thermography)
LH	Left Hand Side
OGV	(Fan) Outlet Guide Vane
PIV	Particle Image Velocimetry
RH	Right Hand Side
TPS	Turbofan Propulsion Simulator
TFN	Through-Flow Nacelle
UHBR	Ultra-High Bypass Ratio (Engine)
VHBR	Very-High Bypass Ratio (Engine)
WT	Wind Tunnel

INTRODUCTION

Background

TPS are used since decades to simulate aircraft engines at wind tunnel model scale [1]. In its simplest form, the representativeness of the full scale conditions is ensured when the same fan nozzle jet efflux velocities are achieved like in the full scale application [2]. Pressurised air turbine driven equipment is used in most practical applications since this technology ensures scalability of power and leaves sufficient headroom for further increments in volumetric power densities. This helps in accommodating the model scale turbine and the shaft inside the model scale volume that houses - at full scale - engine turbomachinery components such as intermediate and high pressure compressors, combustion chamber, turbine and spools. As a consequence of fan jet and geometrical similarities, further characteristics are intrinsically also similar, like fan total pressure ratio, fan rotor blade tip Mach number, specific inlet mass flow rate to mention but a few.

The majority of wind tunnel tests in an aircraft development programme are accomplished with wind tunnel models equipped with passive trough flow nacelles (TFN). Because of higher costs, only a small fraction of tests (so-called "powered tests") are conducted with physical engine simulators.

In order to quantify interferences between the engine and the airframe, it is of particular importance to determine the engine simulator thrust vector to subtract it from the full model balance reactions. In low speed conditions the absolute magnitude of the engine simulator thrust is several times greater than the wind tunnel model airframe drag (same relations as for the full scale aircraft). Consequently, a high thrust determination accuracy is mandatory for determination of drag increments due to interferences between the engine (simulator) and the aircraft (wind tunnel model).

The standard approach is to derive the TPS thrust from gas path measurements of total and static pressures as well as of total temperatures measured in the flow ducts upstream of the propelling nozzles, respectively downstream of the turbomachinery components. A typical conventional setup of the TPS fan duct instrumentation as described in [3] consists of 6 total pressure rakes equipped with 5 Pitot-probes per rake positioned on area weighted radii, 6 static pressure taps at the outer duct wall and 6 total temperature probes. All probes are usually integrated in an instrumentation ring. There is a second instrumentation ring for the core, which is equipped with lesser number of probes/tappings due to the smaller duct size. Fan and core jet velocities are derived from the measurement data. Complementing the measurement data by the fan nozzle size, the fan mass flow rate can be computed. Since the derived parameters based on measurements sampled at discrete positions are not accurate enough, TPS-nacelle-pylon assemblies are calibrated in dedicated engine calibration facilities (ECF's) for fan mass flow rate and thrust.

Future aircraft propulsion systems feature increasing bypass ratios and decreasing fan total pressure ratios (FPR). A consequence is that the level of integration of engine and airframe increases as examples ranging from ultra-high-bypass ratio engines (UHBR) with shortened intakes to boundary layer (BLI) ingestion concepts indicate. It is obvious that intake distortions are a particular challenge for BLI concepts. Numerical and experimental simulations (compare for example [4], [5], [6]) have shown that the intake distortions the fan has to cope with are way higher compared to conventional podded engine nacelles with Pitot-type intake ingesting undisturbed air.

Scope of present work

A key assumption of the calibration and thrust determination approach is that operating conditions of the TPS assembly in the ECF on the one hand and the conditions in the subsequent wind tunnel test on the other hand are similar. This assumption is at risk if the intake distortions vary between calibration and test since it cannot be expected that all distortions are fully smoothed out by the fan stage.

Varying intake distortions and the potential impact on the readings of fixed instrumentation downstream of the fan stage prompt for a more detailed identification of the flow conditions in nominal and deteriorated operation conditions. Rotating rakes moving circumferentially lend themselves as a practical and proven alternative to spatially fixed instrumentation. Fundamental considerations of such equipment are contained in [7], a practical application on engine simulator installed configuration in [8] and an example of rotating rakes equipped with 5-hole probes to measure intake flow swirl with an ejector driven model scale nacelle is described in [9]. Reference [6] describes an application in a BLI wind tunnel test with rotating rake measurements performed ahead and downstream of a fan stage driven by an offset compressed air turbine.

For the wind tunnel test discussed in the present document, following test objectives were pursued:

- Gather experience that allows designing gas path measurement systems with increased robustness w. r. t. changing configurations and operating conditions.
- Identification of the flow characteristics downstream fan outlet guide vanes (OGV's) with particularly emphasis on the fan stator air outlet angles.
- Proof that flow information with high spatial resolution helps to become more independent from the need to reproduce flow conditions of previous calibration runs closely if it comes to thrust determination.

EXPERIMENTAL SET-UP

Wind tunnel

In order to study the effects of varying intake distortions, a wind tunnel test with an isolated TPS-nacelle-pylon setup has been conducted (Figure 1) in Airbus' Bremen Low Speed Wind Tunnel (BLSWT).

BLSWT is an open return wind tunnel with a maximum freestream Mach number of 0.25 and a test section size of 2.1 by 2.1 m (height x width) equipped with an high pressure air supply system for TPS operation.
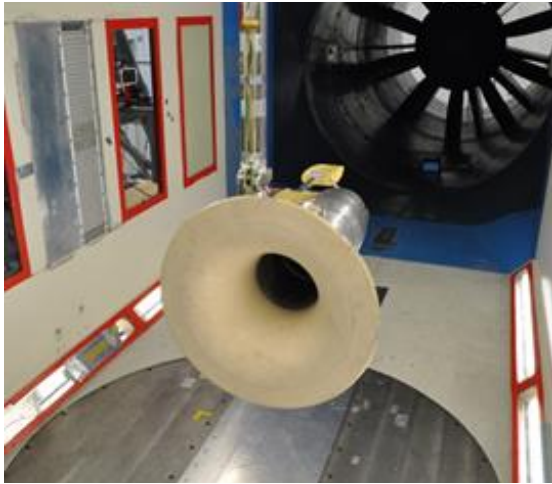
Figure 1: Isolated TPS-Nacelle-Pylon setup in BLSWT. Configuration shown with bellmouth intake / mass flow meter mounted

Turbofan Propulsion Simulator

Key TPS characteristics are listed in Table 1.

Table 1: TPS key characteristics.

Fan	
Fan rotor tip diameter [cm]	15.2
Fan rotor rotation sense[1]	clockwise
Maximum Speed [1/min]	51,000
Mass flow Rate [kg/s]	3.13
Fan Total Pressure Ratio [-]	1.5
Fan Characteristics	VHBR
Turbine	
Drive Air Total Pressure [bar]	40.6
Drive Air Flow [kg/s]	1.15
Power per Shaft [kW]	127

The stator of the single stage fan comprises of a number of 30 OGV's. For the present application it was beneficial that the OGV trailing edges are oriented in radial direction (neither lean nor sweep) as can be seen in Figure 3.

Nacelle and pylon were of conventional design with separate core and fan nozzles. Two intakes have been used, a bellmouth intake ("BM", Figure 1) which functions also as a fan mass flow meter and a conventional drooped 3D TPS Pitot-type intake which is referred to as flight intake ("FI"). The BM intake is equipped with a rotationally symmetric generic representation of a Pitot-type intake with throat and diffuser to ensure that flow conditions provided to the fan are similar to the FI configuration. Intake droop opened the possibility to alter intake conditions by mounting the component in either nominal azimuthal setting

---

[1] Aft looking forward or "pilots view"

(0°) or "upside down" (turned by 180° about the engine axis) to provoke deteriorated intake flow.

Rotating rake system

For detailed mapping of the flow conditions in the fan duct downstream the fan OGV's, the fixed instrumentation ring was replaced by an assembly of two rotating rakes (compare Figure 2) with 5 total pressure probes at different radii as listed in Tab. 2.

Tab. 2: Pitot probe radii.

Probe Designation (xx: 'RH' or 'LH')	Radius [mm]
PTFxx1	72
PTFxx2	67
PTFxx3	61
PTFxx4	55
PTFxx5	48

This setup was complemented by a single total temperature probe on each rake. Static pressures were conventionally measured on the outer duct walls. Both rakes were connected to a geared motor outside the model by arms mounted to a central shaft stub which was suspended by two ball bearings and an articulated shaft equipped with a metal bellow. The actual setting angles were measured with an absolute angle encoder placed on the TPS axis (permanent magnet fixed on TPS non-rotating side, probe mounted opposite on rotating rake central shaft stub). A closed loop control system was used for clocking the rakes.
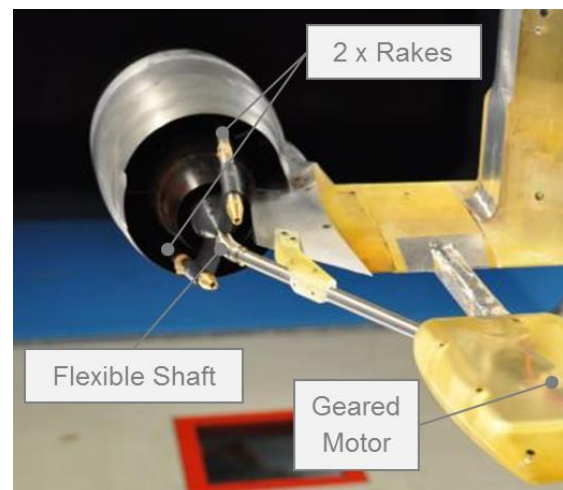

Figure 2: Isolated TPS-Nacelle-Pylon setup with rotating rakes. Configuration shown with flight intake mounted

The rake probe heads were designed to be manually movable in axial direction (see Figure 3, Figure 5 and illustrations in Figure 4) to facilitate measurements in two axial stations of the fan annular duct (1 mm and 16 mm downstream fan

OGV trailing edges) for derivation of local flow angles respectively swirl from OGV wakes.

Figure 3: TPS fan OGV's and rotating rake head in rear axial position

The Pitot-pressures were measured by differential pressure transducers scanners located just outside the wind tunnel. Because the test setup did not allow quick scans of the flow field, data was obtained in pitch and pause mode. The present paper deals with data obtained with 0.5° angle increments. Upper and lower fan duct bifurcations delimited the maximum azimuth angle of rotation to 139.5°.

Data processing and presentation

Only time averaged steady state data was measured in the test campaign. Hence, only steady total pressure distortions have been recorded but no time-variant ('dynamic') data according to the categorization suggested in [12].

All total pressure data are normalised with the freestream total pressure PT0 and fit into a range delimited by a minimum value of unity and a maximum value which is half the TPS design point total pressure ratio.

Test configurations

Different combinations of intake configuration, intake azimuthal settings, angle of attack, TPS speed and fan nozzle size have been tested.

Most of the data presented in the present paper has been obtained for an intermediate corrected rotational speed RPM_{c0} = 30,000 1/min, some for 10,000 1/min.

Corrected speed is obtained from the physical rotational speed and the upstream total temperature:

$$RPM_{c0} = RPM \cdot \frac{1}{\sqrt{\frac{TT0}{T_{ref}}}}$$

FLOW TOPOLOGY IN THE FAN DUCT

Figure 4 provides an overview of the total pressure distributions downstream the OGV trailing edge for a) the forward rake station and b) the rearward rake station. Focussing first on a), following observations can be made:

- High total pressures on the clockwise side of the upper bifurcation.
- Increased total pressures on the counter-clockwise side but not directly next to the upper bifurcation. ⇨ The reason for the low total pressure region on the left hand side of the upper bifurcation was discovered after the test by visual inspection of the fan stator. OGV's with indexes 28, 29 and 30 were twisted such that the average chord line inclination to the TPS axis is less than that of the other vanes. The twist is a flaw that most likely occurred during the joining process of the bladed inner ring with the cylindrical stator housing by brazing. Since the joint gaps are narrow, slight degrees of unbalanced growth or shrinkage of the parts to be joined can cause vane deformation or tear-off at the brazing joints during the cool down phase.
- OGV wakes clearly visible in total pressure contour plots; 24 out of 30 OGV's covered.
- On average the total pressures in the right half of the annular duct are higher than in the left half.
- Total pressures tend to have a radial gradient with higher pressures at bypass duct inner surface and smaller pressures a the duct outer wall.

Now, if the forward rake location a) is compared with the rearward reference location b), the list of observations can be continued:

- The width of OGV wakes increase with distance from the trailing edges.
- Most wakes tend to have shifted their location in counter-clockwise direction except those close to and on the right side of the upper bifurcation.

A more detailed view of the flow topology is provided by Figure 6 with following points:

- Wake depressions are more pronounced in the forward rake compared to the rear rake position.
- The wake deflects from forward to rear location by up to several degrees in both directions from axial flow ($\Delta\theta = 0°$).
- The flow to the right of a minimum is associated with the suction side and the flow to the left of the minimum with the pressure side of a vane.
- A total pressure peak occurs only a few degrees in clockwise direction of a wake minimum that is associated with the suction side of a vane.
- In contrast, the gradient of total pressure increase to the next maximum associated with the pressure side of a vane is significantly smaller.

FAN OGV FLOW ANGLES

Evaluation Approach

Figure 5 shows the concept to determine the air outlet angles α_3 (cascade nomenclature of [11] is used) from the circumferential shift of the OGV wakes $\Delta\theta$, the axial distance ΔD (always fixed to 15 mm) and the radius of the Pitot probes r.

Figure 6 shows the total pressure ratio distribution of the outermost Pitot probe of the right hand side rake in both forward and rear axial positions for the run settings listed in Table 3.

The shift of the minima up to a few degrees in azimuth angle $\Delta\theta$ in both directions can be inferred from mutual comparison of the minima between forward and rear rake positions.

A synoptical analysis of all the data including the total azimuthal total pressure patterns revealed that sudden stepwise changes in the azimuthal location of a small number of vane wakes are unlikely to occur.

$$\alpha_3 = \arctan (\Delta U/ \Delta D)$$
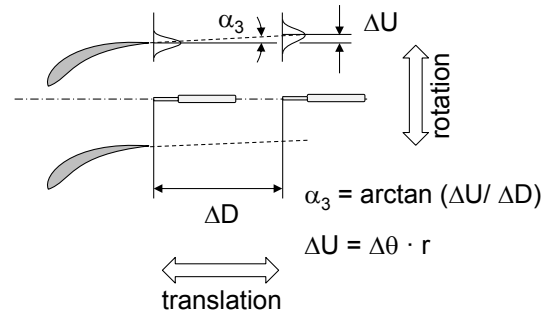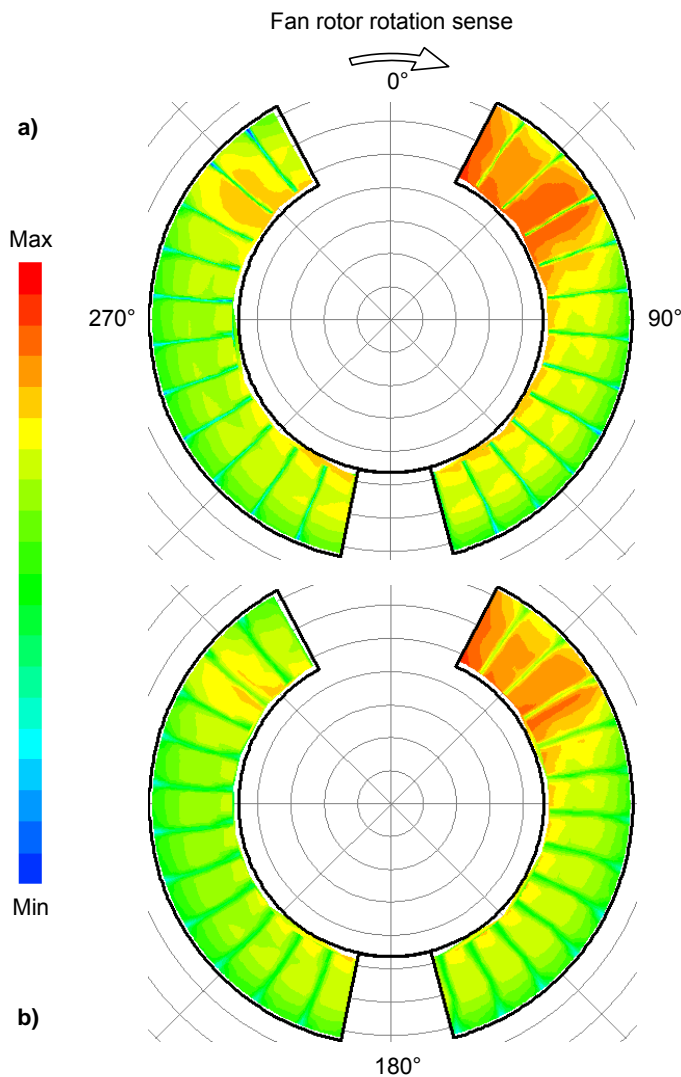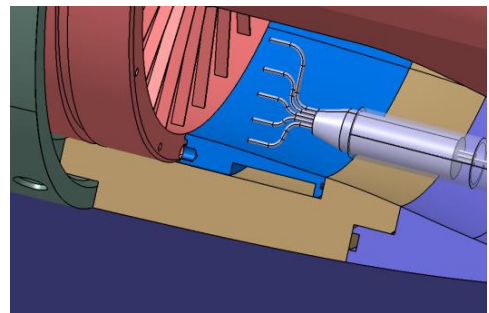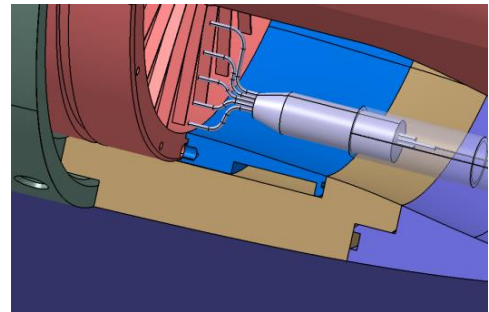$$\Delta U = \Delta\theta \cdot r$$

Figure 5: Concept for fan stator air outlet angle determination from wake surveys in two axial stations.

Figure 4: Fan duct total pressure distribution measured at two different axial stations (flight intake, RPM_{c0} = 30,000 1/min, M0 = 0.2). View: Aft looking forward ("Pilot's view").

27

Hence it was decided to narrow the search region by allocating upper and lower minima search bounds (cyan lines) for each vane.

Table 3: Model configuration and fixed operation parameter settings for Figure 6 through Figure 8.

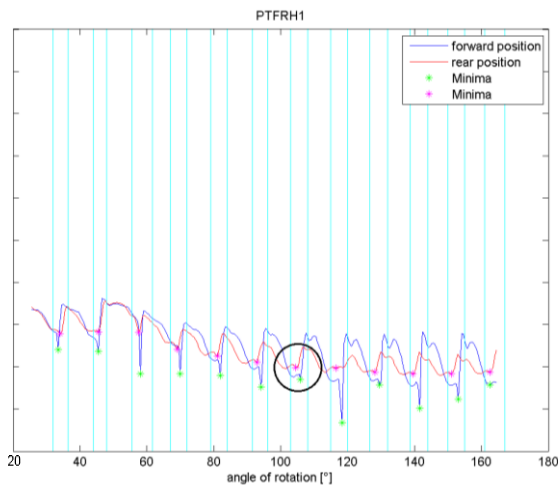| Parameter	Value
Corrected Rotational Speed RPM_{c0}	10,000 1/min
Intake Configuration	Flight Intake
Flight Intake Azimuth Angle	0°
Nozzle Configuration	Large (= Reference)
Angle of Attack α	0°
WT Mach Number M0	0

Figure 6: Total pressure ratio of the outermost Pitot-probe of the right hand side ('RH') rake in the course of two scans in forward and rear locations.

Outlet air angles

Evaluation results in terms of wake deviation angles are depicted in Figure 7 where the outlet air angles α_3 are plotted versus the vane index (or vane number). Please note that adjacent points are connected by dashed lines for better readability. Since the vanes are equally spaced with 12° azimuthal distances to neighbouring vanes, the vane number could be substituted by the azimuth angle θ without changing the plot's appearance. The connecting lines would then be justified when the vane wake deflections are interpreted as representative of the local flow angles.

The data of vane 15 for the outermost radius of 72 mm was insufficient to determine a valid angle. This is for why the data point is missing.

While the deflection angles of vane 4 are positive for all radii, they decrease first steeply such that all deflection angles are negative for vane 6 before decreasing further on average but at a smaller gradient towards the 180° bifurcation.
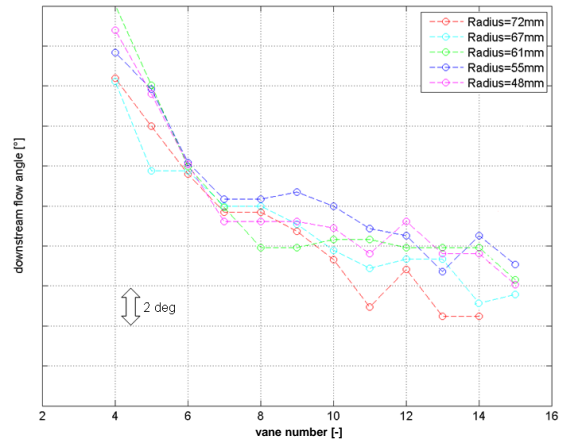

Figure 7: Fan OGV outlet air angles for the right hand side rake.

The span of wake deviation angles from vane 4 to vane 15 is on average approximately 12°. The azimuthal trends are similar for all radii.

It was expected from the outset that the deviations from the optimal flow angles $\alpha_3 = 0°$ are small such that wake locations measured in both axial positions of the rake can be unambiguously allocated to an individual fan outlet guide vane. A wake swap by a single vane count between forward and rear rake positions would require flow angle absolute values of $\alpha_3 = 34°$ for the inner and 45° for the outer Pitot probes. Most outlet air angles deviate consistently throughout the campaign from the ideal 0° figure by single digit degrees. Hence there is no evidence of a wake swap.

In radial direction, all data falls into a span of 4° per vane. Clearly, the azimuthal gradients are higher than the radial ones.

Because of the small radial effects, all five deflection angles per vane have been averaged and are presented for the full annular duct in Figure 8. Flow angles in the left half of the duct (angles for vanes 18 through 28) are all negative (corresponding to a counter-clockwise swirl).
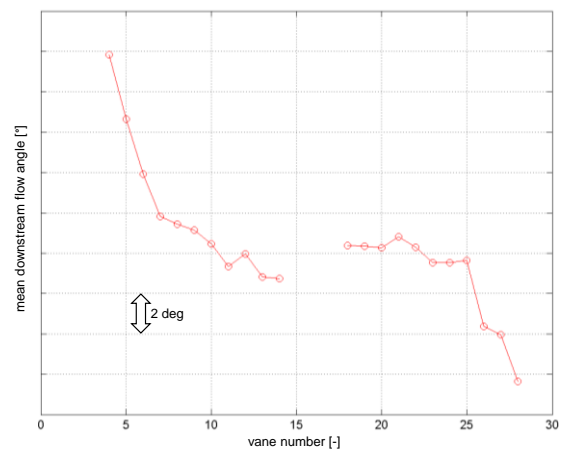

Figure 8: Rake average fan air outlet angles.

Discussion

Starting from an overall average fan air outlet angle it can be observed that the deflection angles steeply increase for the lower vane numbers and that they steeply decrease for the highest ones. This effect can be well explained by displacement of the flow due to the blockage of the flow channel by the upper bifurcation. A similar effect occurs due to the lower bifurcation but the deflections are smaller because the obstruction is less due to smaller axial dimension and circumferential width compared to the upper counterpart.

The overall average of flow angles is several degrees below the optimum value of 0° for axial flow. In other words, the fan stator does not only remove the fan rotor clockwise swirl but induces a counter-clockwise one. It can be speculated that the upper and lower bifurcations help to reduce the swirl in the bypass duct towards the fan nozzle. However, PIV results in Figure 9 from an earlier measurement campaign (without rotating rakes) show that some residual counter-clockwise swirl still persists in the fan jet. Note that contours in Figure 9 only represent the x-velocity component U. Swirl can be inferred from the projections of the velocity vectors depicted as arrows into the Y-Z-plane.
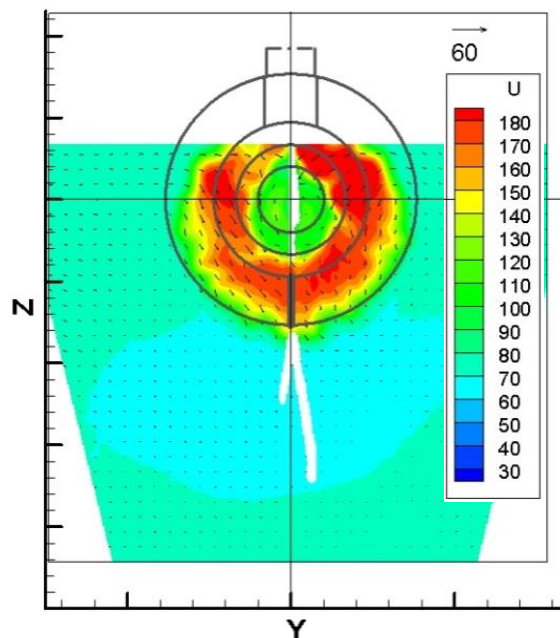

Figure 9: PIV results of isolated TPS configuration: M0 = 0.2, RPM_{c0} = 31500 1/min, PIV-plane 35 mm downstream core plug trailing edge and perpendicular to wind tunnel centre line, nacelle incidence = 2.2°. View: Aft looking forward.

It appears that the vane design trailing edge metal angle was chosen inappropriately. The metal angle of the OGV trailing edges was determined by means of a coordinate measuring machine to α'_3 = -7.5°. While this figure is in line with values suggested by handbook methods [11], the test evidence proofs that the exaggeration angle is actually too high. It is worth to note that Airbus fan stator vane designs feature smaller exaggeration angles around -3°.

Parametric study

An experimental parametric study has been conducted in order to obtain the sensitivities of the fan stator air outlet angles α_3 to variations in the following configuration and operation parameters:

- Fan Nozzle Exit Area: Large (L)|Small (S) NB: S is 8.6% smaller than L
- WT Mach Number M0: 0 | 0.2
- Angle of Attack: 0° | 14.2°
- Intake: Bellmouth (BM) |Flight Intake (FI)
- Flight Intake Azimuth Angle: 0° | 180°

Rake averaged flow angles are shown in Figure 10 for the first three variations and in Figure 11 for the latter two. The diagrams cover corrected rotational speeds of 10,000 1/min corresponding to a fan total pressure ratio of 1.035 (run xx368) and 30,000 1/min corresponding to a fan total pressure ratio of 1.197 (run xx367). While the fan total pressure ratio varies for some of the configuration and operation parameter changes, the figures provide an orientation about the operating state at low and medium rotational speeds of the VHBR TPS.

Effects of parameter variations are generally small when referring to the higher rotational speeds in both figures. This is also true for the lower rotational speeds as the fan nozzle exit area and the angle of attack changes are concerned. Reducing the wind tunnel Mach number to zero while keeping the corrected rotational speed constant affects the air outlet angles α_3 by an increment of up to 2°. A change from flight intake (FI) to the bellmouth intake (BM) has a significant effect on the flow angles at low rotational speed, particularly on the flow in the left half of the annular duct near the lower bifurcation.

The fact that the flow angles are not influenced by the angle of attack is interesting for TPS operated with wind tunnel models of aircraft. The flow angles in the duct do not change from one angle of attack to the other which indicates that the intake provides stable flow to the fan.

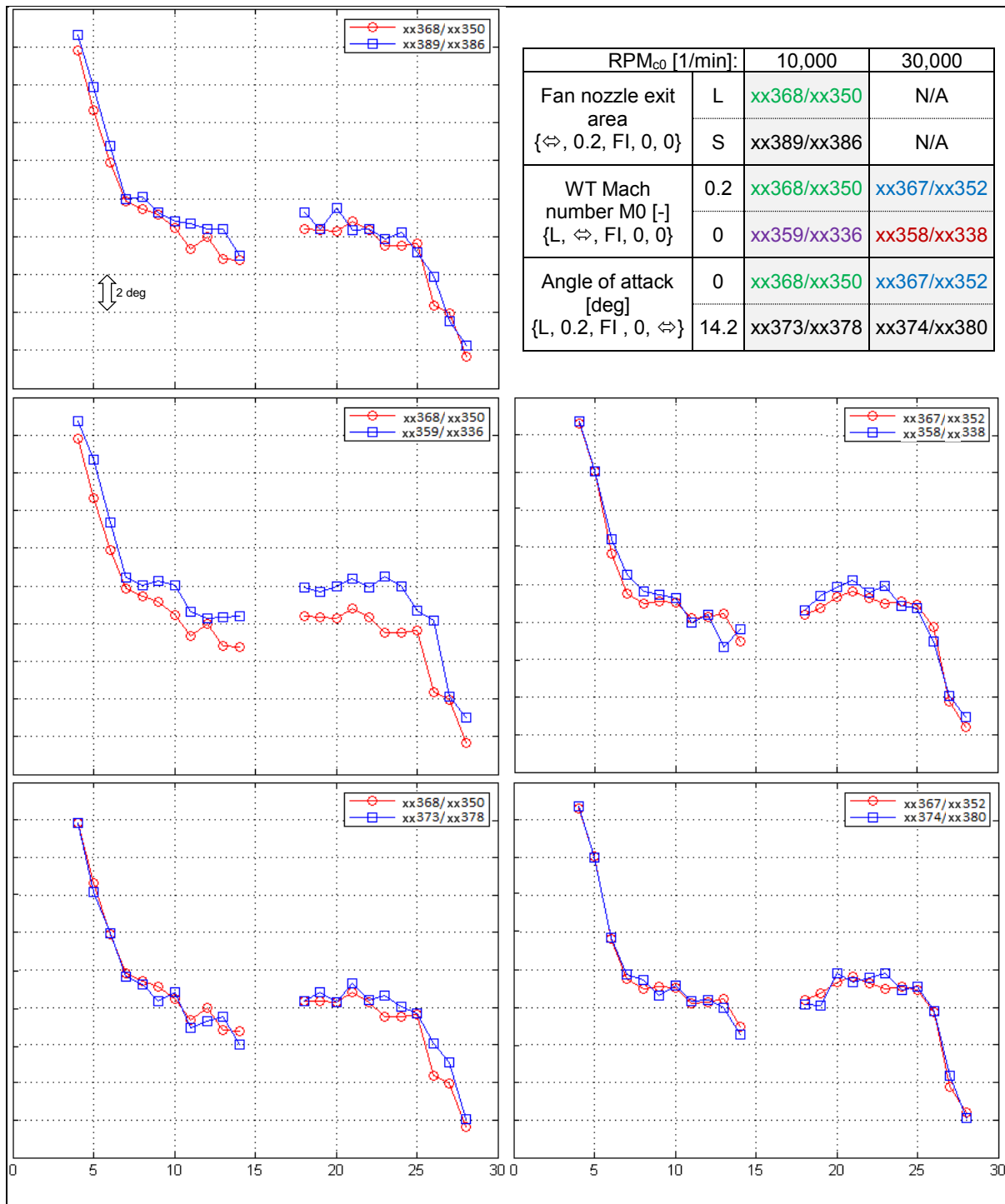| RPM$_{c0}$ [1/min]:		10,000	30,000
Fan nozzle exit area $\{\Leftrightarrow, 0.2, FI, 0, 0\}$	L	xx368/xx350	N/A
	S	xx389/xx386	N/A
WT Mach number M0 [-] $\{L, \Leftrightarrow, FI, 0, 0\}$	0.2	xx368/xx350	xx367/xx352
	0	xx359/xx336	xx358/xx338
Angle of attack [deg] $\{L, 0.2, FI, 0, \Leftrightarrow\}$	0	xx368/xx350	xx367/xx352
	14.2	xx373/xx378	xx374/xx380

Figure 10: Fan OGV air outlet angle variation (ordinates) versus vane index (abscissae) due to changes in fan nozzle exit area, wind tunnel Mach number and angle of attack. Configuration matrix included in upper right hand side cell. Configuration indicated in curly braces: {fan nozzle exit area, WT Mach number, intake configuration, flight intake azimuth angle [°], angle of attack [°]}.

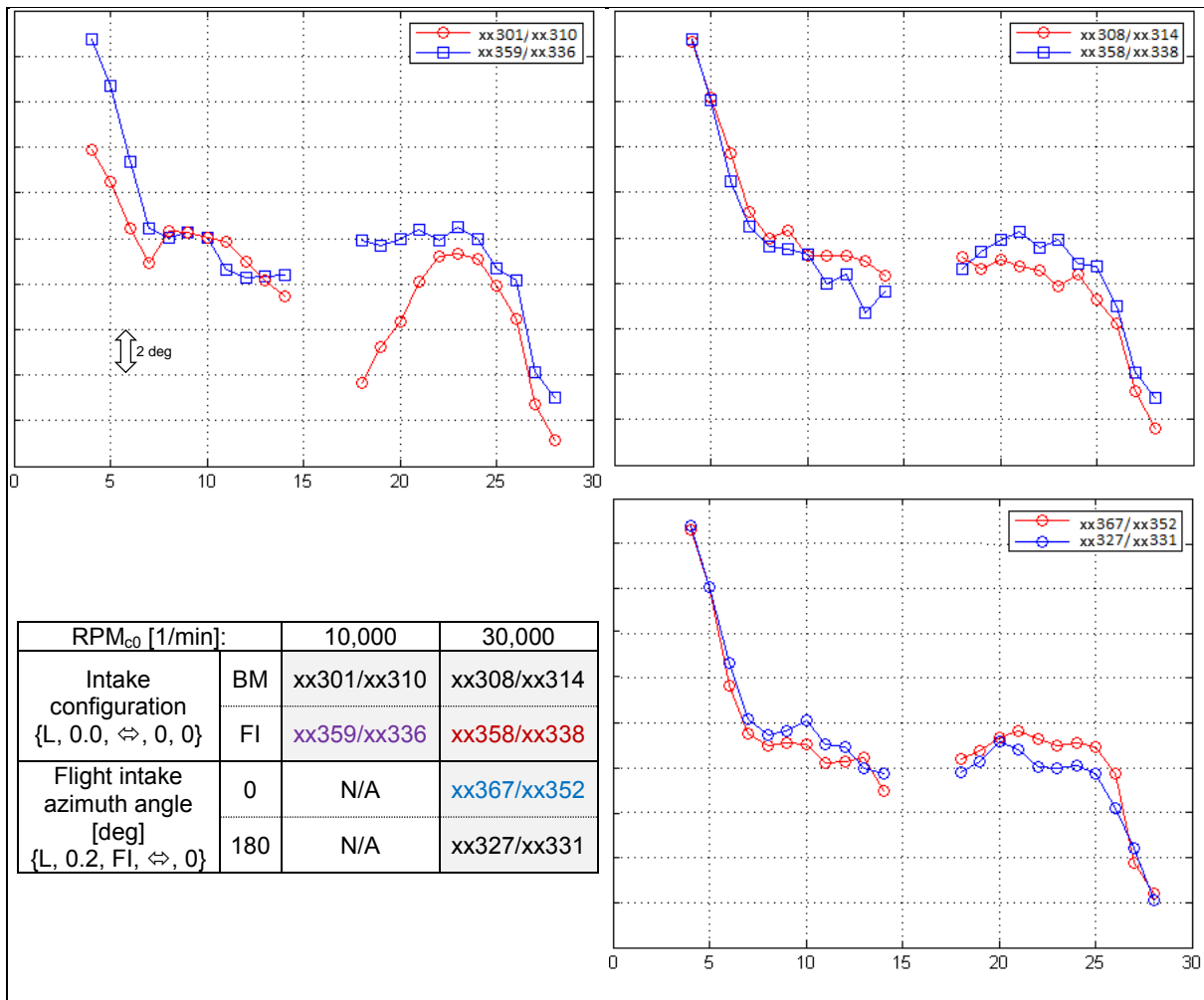| RPM$_{c0}$ [1/min]:		10,000	30,000
Intake configuration {L, 0.0, ⇔, 0, 0}	BM	xx301/xx310	xx308/xx314
	FI	xx359/xx336	xx358/xx338
Flight intake azimuth angle [deg] {L, 0.2, FI, ⇔, 0}	0	N/A	xx367/xx352
	180	N/A	xx327/xx331

Figure 11: Fan OGV air outlet angle variation (ordinates) versus vane index (abscissae) due to changes of intake configuration and flight intake azimuth angle. Configuration matrix included in lower left hand side cell. Configuration indicated in curly braces: {fan nozzle exit area, WT Mach number, intake configuration, flight intake azimuth angle [°], angle of attack [°]}.

THRUST DETERMINATION SENSITIVITIES

Introduction

After having looked at a detailed evaluation of some selected cascade characteristics, some aspects of direct practical relevance shall be addressed in the present section, namely the thrust determination sensitivities w.r.t. the gas path measurements approach. While a selective evaluation was made in the previous section, thrust is obtained by integration of all available gas path measurement data. This can be rephrased in the form of key questions to be answered:

- What benefit can be drawn from a high spatial resolution of the flow field data?
- To what point of adverse flow conditions would a conventional instrumentation layout deliver sufficiently accurate results?

Evaluation approach

Instead of comparing runs performed with rotating rakes on the one hand and further runs made with a conventional fixed rake instrumentation ring test configuration, the available rotating rake information will be evaluated instead using

a) all data of a single flow scan
b) only data obtained at certain azimuthal positions of the rotating rake simulating what would be obtained with a fixed rake instrumentation configuration.

Following standard practice, a configuration comprising of six total pressure rakes is stipulated for b) where the azimuth angles are selected such that the simulated rakes are located amidst two adjacent OGV trailing edges. Table 4 lists the simulated fixed total pressure rake geometrical angles $\theta_{fr,wt}$. They are also depicted by red lines in Figure 12.

31

The corresponding total temperature probe locations are approximately 2° greater than $\theta_{fr,wt}$ for each rake position.

While calibration of fan mass flow rate and TPS thrust is mandatory for practical applications, the subject of calibration will be put aside here because it will have virtually no added value for the discussion. Only a calibrated bellmouth mass flow meter was employed for selected runs at M0 = 0, while reference force data was not obtained in the course of the test campaign at all. Hence only isentropic relations will be evaluated following the lead of [10]. Isentropic in the present context means that the total pressure losses due to the intrusive instrumentation and the bypass duct wall friction and nozzle losses are neglected. Instead the concept suggests that the losses are nil.

Table 4: Simulated fixed rake azimuthal positions.

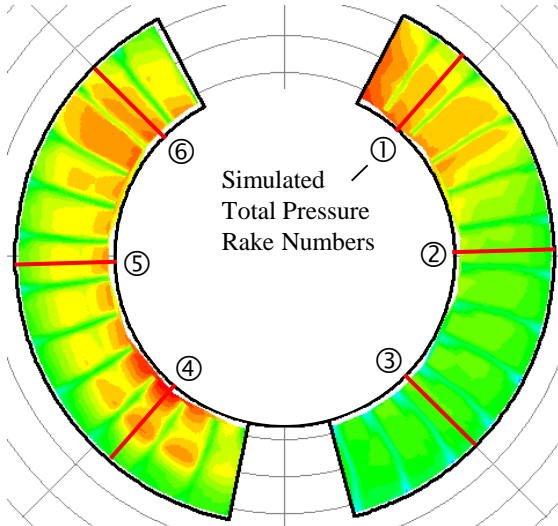| Sim. Tot. Pres. Rake No	$\theta_{fr,wt}$ [deg]
1	40.0
2	88.5
3	135.5
4	220.0
5	268.5
6	315.5

Figure 12: Fixed rake evaluation azimuthal positions $\theta_{fr,wt}$ (indicated by red lines) superimposed to total pressure ratio contour plot of run xx333 (same colorbar as in Figure 4).

Thanks to the area weighted radial distribution of total pressure, the integration across the annular duct reduces to computing the arithmetic mean of all valid data points. For the simulated fixed rake configuration case b) the summed total pressures are divided by the number of (simulated) probes $n_{fix} = 5 \cdot 6 = 30$. For the rotating rake case, a total of 279 recordings were made for 10 total pressure probes at a time. So the integration is made by summing up all pressures and dividing by $n_{rot} = 10 \cdot 279 = 2790$.

Following relations are employed:

- Isentropic fan mass flow rate:

$$DM19is = A19 \cdot \sqrt{\frac{2 \cdot \gamma}{R \cdot (\gamma - 1)}} \cdot \frac{PT15}{\sqrt{TT15}}$$
$$\cdot \left(\frac{P0}{PT15}\right)^{\frac{1}{\gamma}} \sqrt{1 - \left(\frac{P0}{PT15}\right)^{\frac{\gamma-1}{\gamma}}}$$

- Isentropic fan jet velocity:

$$V19is = \sqrt{\frac{2 \cdot \gamma \cdot R}{(\gamma - 1)}} \cdot \sqrt{TT15}$$
$$\cdot \sqrt{1 - \left(\frac{P0}{PT15}\right)^{\frac{\gamma-1}{\gamma}}}$$

- Isentropic fan gross thrust:
$$F19is = DM19is \cdot V19is$$

In order to ease mutual comparisons, mass flow rate and gross thrust are corrected by upstream total pressures/temperatures:

- Corrected isentropic fan mass flow rate:

$$DM19is_{c0} = DM19is \cdot \frac{\sqrt{\frac{TT0}{T_{ref}}}}{\frac{PT0}{P_{ref}}}$$

- Corrected isentropic fan gross thrust:

$$F19is_{c0} = F19is \cdot \frac{1}{\frac{PT0}{P_{ref}}}$$

Analysis of selected run sequences

A run sequence it thought off supporting mutual comparison of test results starting from reference conditions to those where the flow conditions may deteriorate. In the present context configuration and operation parameters are altered in a stepwise manner from settings where optimal fan intake flow conditions can be expected to those where intake total pressure distortions potentially increase up to conditions where boundary layer separations may occur.

Two sequences will be discussed detailed in Table 5 and Table 6. Sequence 1 moves through a typical TPS operational range up to aircraft stall angle of attacks. Runs with indices i = 1 through 3 of Sequence 2 are identical to Sequence 1 but the flow conditions provided to the fan are deteriorated on purpose for 4 and 5 by "upside down" installation of the flight intake.

Table 5: Sequence 1 - Angle of attack range.

i	Run No	Intake Confi-guration	FI Azimuth Angle	α	M0
[-]	[-]	[-]	[deg]	[deg]	[-]
1	xx314	BM	N/A	0	0
2	xx338	FI	0	⇩	⇩
3	xx352	⇩	⇩	⇩	0.2
4	xx380	⇩	⇩	14.2	⇩
5	xx383	⇩	⇩	24.2	⇩

Table 6: Sequence 2 – Deteriorated intake flow.

i	Run No	Intake Confi-guration	FI Azimuth Angle	α	M0
[-]	[-]	[-]	[deg]	[deg]	[-]
1	xx314	BM	N/A	0	0
2	xx338	FI	0	⇩	⇩
3	xx352	⇩	⇩	⇩	0.2
4	xx331	⇩	180	⇩	⇩
5	xx333	⇩	⇩	24.0	⇩

Figure 13 and Figure 14 show evaluations of corrected isentropic fan mass flow rate and corrected isentropic fan gross thrust for Sequence 1. The top subplot (i) depicts the absolute values for both

a) a full integration of the data obtained for a single rotating rakes scan labelled with the subscript "rot" and
b) corresponding values if only the simulated fixed rake positions data is used "fix".

Subplot (ii) below shows increments of runs with indices 2 through 5 with respect to the reference run with index i = 1. Here, the increments in corrected rotational speed are added for reference.

Shown below (iii) is the difference between fixed rake "fix" and rotating rake "rot" data normalised with the latter (hence "fix/rot – 1").

The bottom subplot (iv) finally shows incre-ments of the differences – the percentage changes of the data in the diagram above with respect to the difference "fix/rot - 1" of reference run i = 1.

It worth noting that only data recorded in the rear rake position have been used. Further, the large nozzle configuration applies for all runs. The corrected rotational speed was always 30,000 1/min.

Principal trends in Figure 13 and Figure 14 are similar. Clearly the simulated fixed rake average data of subplot (1) produce approximately 2.4 % higher mass flow and 4.8% higher thrust as subplot (iii) shows. This is to be expected since the low momentum flow regions are purposely omitted for the simulated fixed rake evaluation.
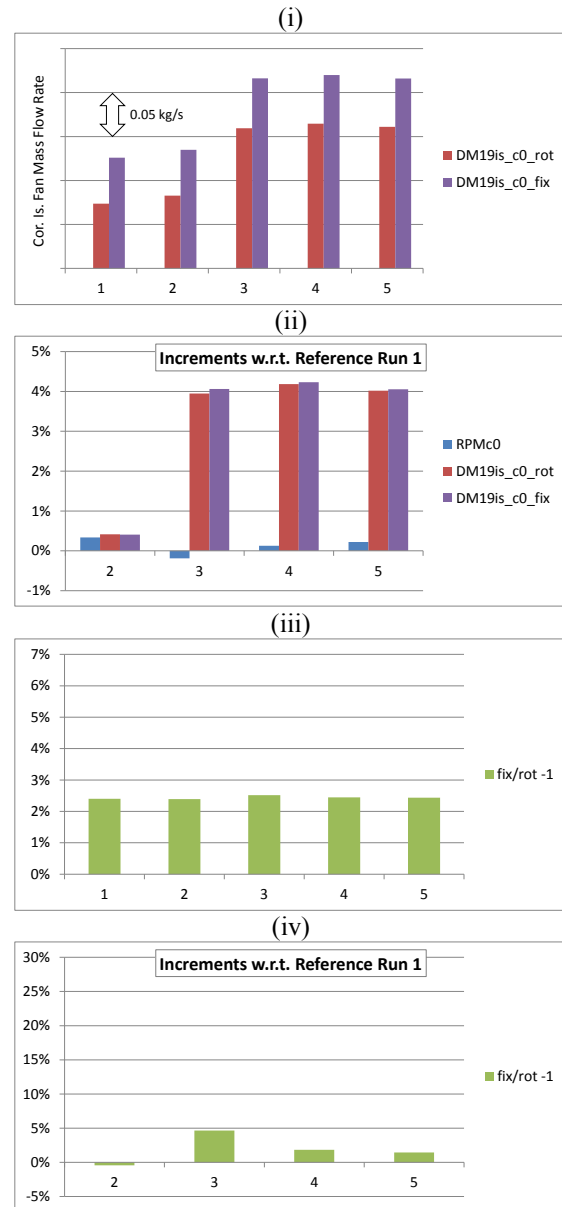

Figure 13: Sequence 1 - Corrected isentropic fan mass flow rate.

After switching from wind-off to wind-on conditions (run 3), mass flow and gross thrust increases significantly because the corrected rotational speed was held constant. Also the flow distribution changes slightly as the approximately 4% difference in subplot (iv) indicates.

Increasing the angle of attack to 14.2° (run 4) and 24.2° (run 5) has no significant further effect which corroborates the validity of the working hypothesis of wind tunnel thrust determination by means of gas path measurement data with fixed rake instrumentation and testifies that the inlet works stably.

Results for Sequence 2 are depicted in Figure 15. While i = 1 through 3 are the same as for Sequence 1, the intake was turned about the engine axis by 180° for i = 4 at zero angle of attack with little difference compared to i = 4 of Seq. 1.
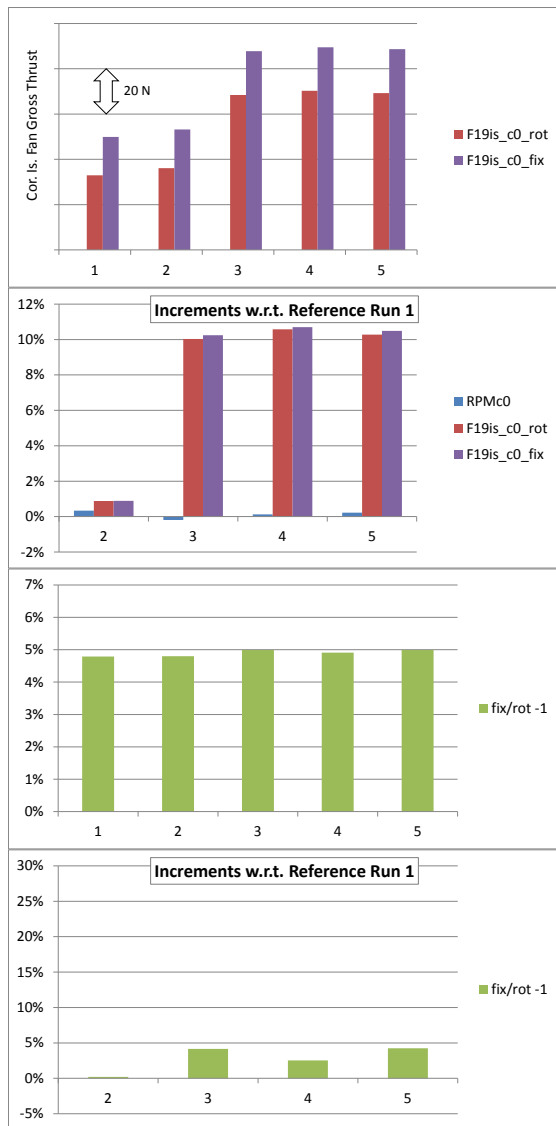
Figure 14: Sequence 1 – Corrected isentropic fan gross thrust.

Figure 15: Sequence 2 - Corrected isentropic fan gross thrust.

When the angle of attack is increased to 24.0° (run 5), the thrust derived from all data "rot" reduces more than that derived from the fixed rake locations "fix".

Making the reasonable assumption that the integrated detailed flow data is more representative of the actual flow conditions compared to the selective spatial sampling of the simulated fixed rake configuration, the thrust $F19is_{c0}$ would be overestimated by approximately 1% if a conventional fixed rake configuration would be used. This offset compares with an empirical standard error estimate of 0.2% (2·s, 95% confidence level) for Sequence 1.

Infrared images have been recorded with an IR camera in the course of run xx333 ($\Rightarrow$ Sequence 2 i = 5). A still image of the inner side of the lower intake lip in original and post-processed versions are depicted in Figure 16 and proof that the intake inner flow was partly separated.
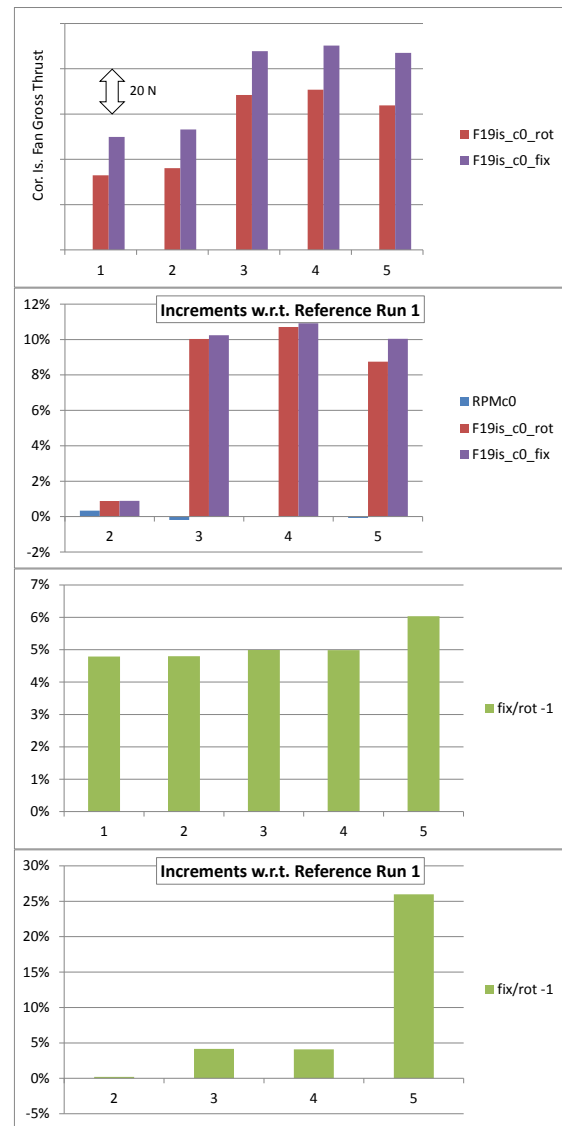
The effect of the deteriorated intake flow on the conditions downstream the fan stage can also be clearly seen in the total pressure ratio contour plot Figure 12.
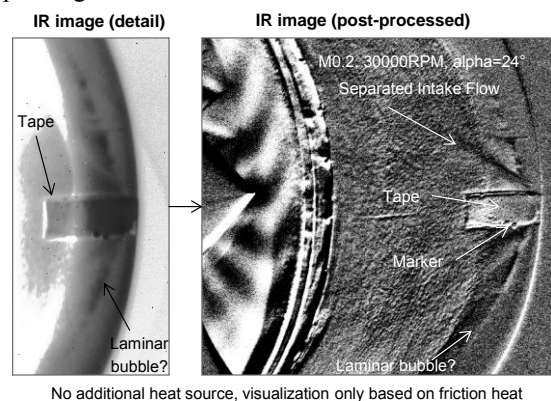

No additional heat source, visualization only based on friction heat

Figure 16: Infrared images of "lower" intake lip with intake mounted azimuthally turned by 180° to provoke intake flow separation.

34

CONCLUSIONS

An experimental parametric study into the flow characteristics downstream of a TPS fan stage installed in a strut supported isolated nacelle-pylon configuration has been performed in a low speed wind tunnel. The sensitivity of stator outlet flow angles and the impact of spatial resolution on gas path measurements derived isentropic mass flow rates and gross thrusts to configuration and operation parameter variations have been studied with the following findings:

- TPS fan OGV outlet air angles can be accurately determined from OGV wake data obtained with rotating Pitot probe rakes traversed circumferentially at two different axial distances from the OGV trailing edges.

- The fan air outlet angles are insensitive to changes in configuration and operation parameter changes. The smaller the fan total pressure ratio, the greater the effects. It was found that a change of the intake configuration from bellmouth to flight intake has the greatest effect.

- It was found that the exaggeration angle of the fan outlet guide vanes of -7.5° is not suitable as to guarantee purely axial flow downstream the fan stage. An angle of -3° would be more appropriate for the stator design studied.

- A classical six Pitot probes rake configuration provides sufficient flow information for nominal flight intake range applications.

- High spatial resolution of flow data makes data reduction more robust against flow deterioration and varying distortions of fundamental flow quantities. Recording of highly spatially resolved flow data hence lends itself for applications where flow distortions are likely to significantly change from reference condition values.

A substantial benefit of employing rotating rakes is to be expected for tests where high angle of attacks are investigated close to the intake aerodynamic design limits and beyond as well as tests with BLI configurations.

Future enhanced rotating rake systems are to be developed towards higher data acquisition rates in order to increase test productivity. Modular concepts would be desirable, that permit exchanges of rakes and/or probes. For instance, it would be an advantage to have the possibility to change from Pitot's to probes providing the local velocity vector, e.g. 3- or 5-hole probes.

ACKNOWLEDGMENTS

REFERENCES

[1] Burgsmüller, W.; Castan, C.; Hoheisel, H.; Kooi, J. W.; 1995. "Preparation and Use of TPS-Technique for Low Speed Investigations on Transport Aircraft", Proceedings of International Forum on Turbine Powered Simulation, DNW, 16/17 May 1995

[2] von Schweppenburg, H. F. G.; 2005. "Ein Verfahren zur genauen Schubbestimmung von Modelltriebwerken im Windkanal", DLR-Forschungsbericht 2004-26

[3] John, R.; 1995. "TPS Units to Meet Future Requirements – Simulation of Very High Bypass Ratio Engines", in proceedings of International Forum on Turbine Powered Simulation, DNW, 16/17 May 1995

[4] Plas, A. P. et. al.; 2007. "Performance of a Boundary Layer Ingesting (BLI) Propulsion System, AIAA 2007-450, presented on 45th AIAA Aerospace Sciences Meeting and Exhibit, 8-11 January 2007

[5] Schönweitz, D.; Nicke, E.; Schnell, R.; Mennicken, M.; 2017. "Fan Design for Boundary Layer Ingestion", New Engine Integration Concepts Symposium, TU-Braunschweig, 23. - 24.08.2017

[6] Arend, D. J., et. al.; 2017. "Experimental Evaluation of an Embedded Boundary Layer Ingesting Propulsor for Highly Efficient Subsonic Cruise Aircraft", AIAA 2017-5041, presented on 53rd AIAA/SAE/ASEE Joint Propulsion Conference, 10-12 July 2017

[7] Saravanamuttoo, H. I. H. (ed.); 1990. "Recommended Practices for Measurement of Gas Path Pressures and Temperatures for Performance Assessment of Aircraft Turbine Engines and Components", AGARD-AR-245

[8] Lieu, M.; Uranga, A.; Drela, M.; Greitzer, E.; 2014. "Rapid Flow Surveys via Rotating Rake System and Use in Powered Wind Tunnel Models", AIAA 2014-2801, presented on 30th AIAA Aerodynamic Measurement Technology and Ground Testing Conference, 16-20 June 2014

[9] Dickey, E. D.; Princen, N. H.; Bonet, J. T.; Ige, G. K.; 2016. "Wind tunnel Model Design and Fabrication of a 5.75% Scale Blended-Wing-Body Twin jet Configuration", AIAA 2016-0008, presented on 54th AIAA Aerospace Sciences Meeting, 4-8 January 2016

[10] Rowe, R. K.; 1982. "Nozzle performance calibration and turbomachinery operational analysis of Turbo-Powered Simulators (TPS) for the NASA-Langley EET propulsion airframe integration investigation", Final Draft, Contractor Report NAS1-15345, January 1982

[11] Saravanamuttoo, H. I. H., et. al.; 2009. "Gas Turbine Theory", 6th ed., Pearson Education Limited

[12] Seddon, J.; Goldsmith, E. L.; 1999. "Intake Aerodynamics", 2nd ed., AIAA Education Series